Design and analysis of air acoustic vector-sensor configurations for two-dimensional geometry

Mohd Wajid, Arun Kumar, and Rajendar BahlMRB

Citation: J. Acoust. Soc. Am. **139**, (2016); doi: 10.1121/1.4948566
View online: http://dx.doi.org/10.1121/1.4948566
View Table of Contents: http://asa.scitation.org/toc/jas/139/5
Published by the Acoustical Society of America

Design and analysis of air acoustic vector-sensor configurations for two-dimensional geometry

Mohd Wajid,[a] Arun Kumar, and Rajendar Bahl
Centre for Applied Research in Electronics, Indian Institute of Technology Delhi, New Delhi 110016, India

(Received 22 July 2015; revised 6 April 2016; accepted 12 April 2016; published online 17 May 2016)

Acoustic vector-sensors (AVS) have been designed using the P-P method for different microphone configurations. These configurations have been used to project the acoustic intensity on the orthogonal axes through which the direction of arrival (DoA) of a sound source has been estimated. The analytical expressions for the DoA for different microphone configurations have been derived for two-dimensional geometry. Finite element method simulation using COMSOL-Multiphysics has been performed, where the microphone signals for AVS configurations have been recorded in free field conditions. The performance of all the configurations has been evaluated with respect to angular error and root-mean-square angular error. The simulation results obtained with ideal geometry for different configurations have been corroborated experimentally with prototype AVS realizations and also compared with microphone-array method, viz., Multiple Signal Classification and Generalized Cross Correlation. Experiments have been performed in an anechoic room using different prototype AVS configurations made from small size microphones. The DoA performance using analytical expressions, simulation studies, and experiments with prototype AVS in anechoic chamber are presented in the paper. The square and delta configurations are found to perform better in the absence and presence of noise, respectively. © *2016 Acoustical Society of America*.
[http://dx.doi.org/10.1121/1.4948566]

[MRB] Pages: 2815–2832

I. INTRODUCTION

An acoustic vector-sensor (AVS) measures the acoustic pressure as well as the acoustic particle velocity, which can be used to estimate the acoustic intensity vector. Assuming a single acoustically radiating source in the field, the acoustic intensity vector ideally points from an acoustically radiating source to the direction of the AVS device. Acoustic intensity can be used for sound power determination, sound source direction estimation, sound source identification, etc. The acoustic intensity vector is a product of the acoustic pressure (scalar quantity) and the acoustic particle velocity, and is a measure of the acoustic energy flow rate per unit normal area perpendicular to the direction of the flow, its unit being Watt per square meter (W m^{-2}).[1–4] The particle velocity is the average of alternating velocities of the oscillating particles of the medium caused by the acoustic wave.[5] Practically, an AVS can be designed using one of the two methods, namely, the pressure-velocity (P-U) method and the pressure-pressure (P-P) method. In the P-U method, the particle velocity is obtained either by time integration of the accelerometer measurements or by direct measurement such as using an anemometer or double hot-wire sensor called Microflown.[6–8] A typical P-U based AVS device consists of a pressure sensor and a three-channel acoustic particle velocity/accelerometer sensor giving the velocity/acceleration components in the three orthogonal directions. In the P-P method, the particle velocity is calculated using finite difference (FD) approximation of the spatial derivative of the sound-field. It requires that the separation d between the two microphones should be much smaller compared to the acoustical wavelength, λ. Generally, for obtaining good accuracy in the intensity measurement of an acoustic monopole, FD errors are minimized by employing the smallest possible values of d/λ and d/r, where r is the range of the sound source, assuming a single source.[9,10] As the microphone separation d increases for the fixed frequency, the approximation of the measured pressure-gradient will deviate from the true pressure-gradient value at the geometric center of the microphones. The FD approximation method is sensitive to sensor noise, microphone mismatch, reflection and diffraction of the source radiated signal, placement of the microphones, the structure that holds the microphones and the polar pattern characteristics of each microphone. As the source frequency increases, reflections from the microphone body, connecting wires, and the supporting structure also increase, thus partially blocking the propagation of the acoustic waves. At low frequencies, when the wavelength is large compared to the separation between the closely spaced microphones, the small phase difference between the signals impinging on them may be significantly affected due to electrical phase mismatch of the microphones. This may cause error in the pressure-gradient measurement and hence the particle velocity.[1,4,11] A typical P-P based AVS device has closely spaced omni-directional and/or gradient-microphones that measure the pressure and pressure-gradients in the three orthogonal directions which are used for particle velocity estimation.[11] Thus, the output of an AVS consists of four channels, namely, the acoustic pressure $p(t)$ and the three Cartesian components of the particle velocity, denoted by $v_x(t)$, $v_y(t)$, $v_z(t)$.

In this work, we have identified and compared the two-dimensional (2-D) direction-finding capability of different planar AVS configurations implemented using small size omni-directional microphones, and assuming a single source.

[a]Electronic mail: crz118350@care.iitd.ac.in

There are various applications of direction-finding of acoustic sources such as in automatic steering of a camera toward the direction of a speaker in an auditorium, vehicle localization and monitoring systems, detection of non-line-of-sight battlefield target, intensity based sound source separation, hands-free mobile communication, etc.[12–15] In microphone-array based direction-finding, the separation between two neighboring microphones in a uniform linear array (ULA) is required to be less than half of the minimum wavelength in order to avoid spatial aliasing[16] and the angular resolution in the far-field is inversely proportional to the aperture size, measured in the units of wavelength. Alternatively, an AVS can perform spatial processing with a compact arrangement of microphones in contrast to conventional microphone-array which requires wide spacing between the microphones.[17] Several direction-finding applications can benefit from the comparatively smaller size of an AVS. An AVS based direction-finding method is less sensitive to the range of the source,[18,19] able to reject the noise or interference sources selectively with a very small aperture[12,20] and mostly requires fewer data acquisition channels.[21] It has been reported that AVS based direction-finding is relatively more robust in a reverberant environment than those based on time-delay of arrival (TDoA), subspace and steered response power method.[22] The secondary reflections in a reverberant environment are reduced in an AVS due to co-location of the sensors and the directionality of the sensor.[23] The TDoA-based methods require large baseline and are not accurate for closely spaced sensors in a microphone-array. Also, the microphone-array methods are computationally expensive due to the peak search requirements. In the case of a single source, high SNR, and free field condition, the intensity based direction of arrival (DoA) estimation method has the advantages of simplicity of implementation and not requiring a search as in the case of microphone-array based DoA estimation. The improvement in speech de-reverberation using AVS compared to ULA has been reported for a highly reverberant environment.[24]

The purpose of this paper is to conduct a systematic analysis of the P-P based AVS design using omni-directional microphones and compare different AVS configurations for DoA estimation in the absence and presence of uncorrelated noise. The investigation of various planar configurations of omni-directional microphones for intensity based DoA estimation and their performance comparison is reported. The mathematical analysis, finite element method (FEM) numerical simulation considering zero-size as well as non-zero size microphones, and experiments using constructed prototype AVS in full-anechoic room are discussed. The vector-sensor configurations with optimum performance are also compared with microphone-array based direction-finding methods like Multiple Signal Classification (MUSIC) and Generalized Cross Correlation (GCC). Further, the effects of microphone-separation, signal-to-noise ratio (SNR) and signal-duration are also investigated for DoA estimation for the different AVS configurations. It has been observed that increasing the signal duration from 25 to 1000 ms has no improvement on the performance of the DoA estimate in the absence of noise for all the AVS configurations considered. The delta and star configurations are better than the other AVS configurations in the presence of uncorrelated additive noise, however in the absence of noise the sub-configurations of the square configuration give a better DoA estimate. Also, the rate of increase in error for delta and star configurations with respect to microphone separation is less than the other configurations considered. Amongst delta and star configurations, the delta configuration may be preferred as it uses fewer number of microphones than star configuration.

The paper is organized as follows. In Sec. II, the prior art on design and DoA algorithms for AVS are discussed. In Sec. III, a brief background of intensity measurement methods and determination of DoA is presented. In Sec. IV, we give the mathematical expressions of acoustic intensity for several geometrical configurations of omni-directional microphone based AVS for DoA estimation. Section V deals with the numerical simulation setup, their results, observations, and comparisons with standard microphone-array methods. In Sec. VI, the experimental setup in a full anechoic room for AVS prototype, non-zero size microphone simulation and their results for DoA estimation are given. Finally, Sec. VII concludes the work.

II. PRIOR ART IN DESIGN AND DOA ALGORITHMS FOR AVS

The research literature on the design of air AVS including the optimal placement of the component sensors is quite limited. A 3-D intensity probe design for broad frequency band is reported by Miah and Hixon,[4] where seven omni-directional microphone based arrangement is presented consisting of two-concentric orthogonal arrays. They have used smaller separation between the microphones for high frequency band (1.0–6.5 kHz) and larger separation between the microphones for the low frequency band (200 Hz to 1.0 kHz). However, the motive is only to measure the total acoustic intensity and its performance for DoA estimation is not evaluated. Nagata *et al.*[25] have demonstrated a rotating acoustic intensity measurement system consisting of three pairs of matched and variable directional microphones for removing the effects of phase mismatch and position error. They also tried to address the issues related to a two-microphone probe, which may not be directed accurately toward the sound source while measuring sound field parameters. This system is used in determining the maximum acoustic intensity, beam-width of major lobe, peak acoustic intensity of minor lobes, sound source identification, sound power determination, and sound source direction estimation. The null search method is used for source direction estimation where rotation of the microphone probe is required. However, there is no detailed study and results are presented for source direction estimation for the given design. Shujau *et al.*[11] have designed an AVS using an offset-orthogonal arrangement of three pressure-gradient microphones and an omni-directional microphone. The MUSIC algorithm is applied on the pressure-gradient microphone signal for DoA estimation. This AVS design reduces the effect of shadowing and reflection of the signal in 1 to 10 kHz band, due to the microphone body and its supporting structure as compared to the AVS given by Lockwood and Jones.[21] The average

angular error is reported to be on the order of 2° for a range of frequencies. Craven and Gerzon[26] have proposed a coincident microphones arrangement, where four directional microphones are placed on the four surfaces of the tetrahedron. The linear combination of these microphone signals is used to yield directional characteristic of the sound field. Gunel *et al.*[13] have used a non-planar arrangement of four microphones to generate the B-format signal and thereby calculate the intensity vector. Thereby, the direction of sound sources for separation of convolutive mixture is estimated, but the DoA estimation accuracy is not presented. A P-U based AVS quad consisting of four microphones and 12 particle velocity sensors has been used to estimate the DoA of a source at 45° in an anechoic room, and the angular errors reported are 3.7°, 2.8°, 1.2°, and 0.6° for four different algorithms.[27] However, the results for other than 45° direction of arrivals are not reported in detail. An algorithm for improving the particle velocity and intensity measurement for the P-P method is given by Bai *et al.*,[1] but the proposed approach assumes that the direction and the location of the sound source are known *a priori*.

Nehorai and Paldi[28] have derived the Cramer-Rao bound for the estimation of angular error using AVS array where all source signals are assumed to be zero mean, identically distributed and independent of each other. They have also proposed two DoA algorithms using single AVS, one based on the intensity vector, and the other based on only the particle velocity, and their performance is evaluated in terms of mean square angular error (MSAE). Further, Hawkes and Nehorai[29] proved that the intensity vector based DoA estimator capability can be considerably enhanced in ambient isotropic-noise compared to the case of spatially uncorrelated noise. A maximum likelihood-based DoA algorithm in the presence of isotropic noise for a single vector-sensor is presented by Levin *et al.*,[30] where one monopole and three orthogonally arranged dipole receivers have been used, but it has been assumed that the monopole and dipole beampatterns are ideal. The effect of reverberation for DoA estimation performance using an ideal model of AVS is examined and simulated by Levin *et al.*,[31] in which it has been claimed that an intensity-based DoA estimator produces biased results in a reverberant environment and this bias is dependent on the room impulse response (RIR) which is deterministic in nature. In all the above literature, the angular error due to pressure-gradient approximation is not considered, and it has been assumed that the AVS design is ideal, i.e., there is no error in measuring the particle velocity and intensity. A low computation DoA algorithm based on principal component analysis (PCA) of particle velocity has been developed under ambient noise and room reverberant environment, but it uses a large number of spherical microphones and assumes diffused reverberation which is not typical in a practical scenario. It also does not consider sensor noise which causes deviation from the actual DoA. The results show that the DoA estimator is not significantly affected by decreasing SNR from 20 to 0 dB, i.e., because of the ambient isotropic-noise consideration.[22] Tam and Wong[32] presented the mathematical analysis on direction-finding accuracy due to non-idealities in AVS gain response, phase response, spatial dislocation, and non-orthogonal orientation of velocity sensors. A technique for improving direction-finding when the orientation of an AVS is time-varying, is presented by Yuan.[33] The lower-bound on the DoA estimation error variance has been derived by Song and Wong[34] when an ideal AVS is subjected to a velocity-sensor component breakdown. Hochwald and Nehorai[35] have shown that two number of acoustic sources, that are not fully correlated, can be identified using a single AVS when second order statistics is used.

In most of the prior art, only orthogonal arrangement of microphones is considered and other configurations of microphones for P-P based AVS design are not studied for DoA estimation. Also, there is no comparative study amongst the different microphone configurations for DoA estimation using acoustic intensity. In the present work, we have studied several possible geometrical arrangements of microphones for P-P based AVS design and their results for 2-D DoA estimation are studied and compared.

III. ACOUSTIC INTENSITY AND DOA

The relation between the particle velocity and the pressure-gradient at a point location with position vector $\mathbf{r}$ in 1-D for any time t is given by the linearized Euler equation,

$$\frac{\partial p(\mathbf{r},t)}{\partial x} = -\rho_0 \frac{\partial v_x(\mathbf{r},t)}{\partial t}, \tag{1}$$

where ρ_0 is the density of the medium, v_x and p are the particle velocity component along the x axis and pressure at a specified point $\mathbf{r}$ and time t, respectively. The particle velocity at a fixed location is estimated by using the FD approximation of the pressure-gradient. The pressure-gradient is derived from a pair of well-matched (in magnitude and phase) omni-directional microphones placed along the x axis and separated by a distance d as shown in Fig. 1. The FD estimated particle velocity[4,10] along the line joining the two microphones on the x axis in this case, is given by

$$v_x(t) \backsimeq -\frac{1}{\rho_0}\int_{-\infty}^{t} \frac{p_2(\tau)-p_1(\tau)}{d}\,d\tau, \tag{2}$$

where $p_1(\tau)$ and $p_2(\tau)$ are the pressure waveform realizations of wide sense stationary ergodic random processes. The instantaneous intensity $\mathbf{I}(t)$ of an acoustic wave is obtained as the product of the pressure and the particle velocity at the same location.[31] For a fixed location, the instantaneous intensity component along the line joining the two microphones, i.e., the x axis is given by

$$I_x(t) = p_x(t)v_x(t), \tag{3}$$

where $p_x(t)$ is approximated by the average of the two pressure signals $p_1(t)$ and $p_2(t)$. The intensity component I_x along the x axis, is the time-average of the acoustic intensity for steady state sound field

$$I_x = \lim_{T\to\infty}\frac{1}{T}\int_0^T p_x(t)v_x(t)dt. \tag{4}$$

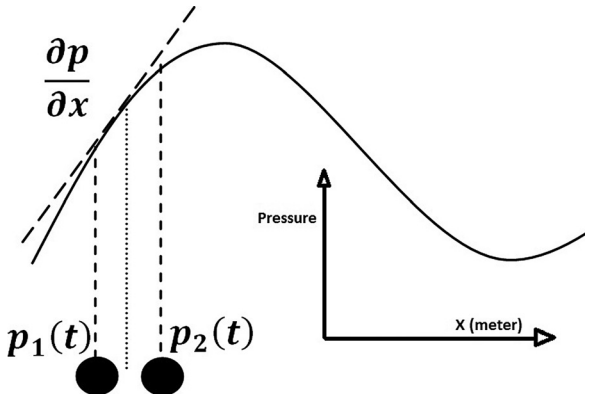

FIG. 1. Approximation of the pressure-gradient of an acoustic wave using two pressure measurements, p_1 and p_2, from two omni-directional microphones (indicated by circles) separated by a distance, d ($d \ll \lambda$).

The average intensity along the x axis, can be written as

$$I_x = \int_0^\infty I_x(\omega) d\omega, \tag{5}$$

where $I_x(\omega)$ is the intensity spectrum and is given as

$$I_x(\omega) = \frac{1}{\omega \rho_o d} \mathrm{Im}\left(\Gamma_{p_1 p_2}(\omega)\right), \tag{6}$$

where $\Gamma_{p_1p_2}(\omega)$ is the cross power spectral density (CPSD) of the two measured pressure signals, $\omega = 2\pi f$ and Im(*) indicates the imaginary part of the argument.[4,9,12,36–38] Similarly, for n number of closely spaced microphones having position vectors $\mathbf{r_1}, \mathbf{r_2}, \ldots, \mathbf{r_n}$, there will be $n(n-1)/2$ number of microphone pairs, so the $n(n-1)/2$ number of intensity vectors $\mathbf{I_{qij}}$ are aligned along the vectors $\mathbf{q_{ij}} = \mathbf{r_i} - \mathbf{r_j}$ $\forall\, i = 1$ to n and $j = i+1$ to n. These intensity vectors are projected on the two orthogonal axes and the average intensity components are given by

$$I_x = \frac{2}{n(n-1)} \sum_{i=1}^{n} \sum_{j=i+1}^{n} I_{qij,x} \tag{7}$$

and

$$I_y = \frac{2}{n(n-1)} \sum_{i=1}^{n} \sum_{j=i+1}^{n} I_{qij,y}, \tag{8}$$

where $I_{qij,x}$ and $I_{qij,y}$ are the projections of $\mathbf{I_{qij}}$ on the orthogonal axes. These average intensity components are used to obtain the DoA of the radiating source in 2-D using

$$\hat{\theta} = \tan^{-1}\left(\frac{I_x}{I_y}\right), \tag{9}$$

where θ is the DoA estimate with respect to the y-axis. This DoA estimation approach is referred as arc-tangent based method. The average intensity component is useful when a single source is present in the field. If multiple sources having non-overlapping frequency bands are present, then the DoA can be obtained as a function of source frequency using,

$$\hat{\theta}(\omega) = \tan^{-1}\left[\frac{I_x(\omega)}{I_y(\omega)}\right], \tag{10}$$

where $I_x(\omega)$ is obtained using Eq. (6) and similarly $I_y(\omega)$ is obtained along the y-axis.

IV. ANALYSIS OF AVS CONFIGURATIONS FOR DOA ESTIMATION

Several P-P based AVS designs using different microphone configurations have been investigated in this paper. The microphone configurations studied are the star, delta, three-microphone obtuse angle configuration (OAC), and square configuration along with its sub-configurations as shown in Fig. 2. The comparisons of DoA estimation of an acoustic source are made between different AVS configurations and expressed in terms of the power spectral density (PSD) of pressure signals for the far field single source. In this paper, all the angles of arrivals are measured clockwise with respect to the y-axis. For each AVS microphone configuration, the intensity vectors are calculated along the solid lines joining the pairs of microphones. These are used to estimate the average intensity components I_x and I_y as given in Eqs. (7) and (8). In the following subsections, $\alpha(\omega)$ is the attenuation factor at the angular frequency ω, and $\tau_{i,j}$ is the time delay of arrival between the ith and jth microphones for a plane wave propagating along the unit vector $\mathbf{a}$, and is given by

$$\tau_{i,j} = \frac{\mathbf{a}^T(\mathbf{r_i} - \mathbf{r_j})}{\kappa}, \tag{11}$$

where $\mathbf{r_i}$ and $\mathbf{r_j}$ are the position vectors of the ith and jth microphones, respectively, and κ is the speed of sound in air.

A. Star configuration

The star configuration consists of four microphones as shown in Fig. 2(a). In this configuration, three intensity vectors are formed aligned with the solid lines. Let $p_c(t)$, $p_k(t)$, $p_l(t)$, and $p_m(t)$ be the pressure signals recorded using the four microphones of the star configuration. Using Eq. (8), the average intensity component for the star configuration along the y-axis is given by

$$\begin{aligned} I_y^{\mathrm{star}} = &-\frac{1}{3\rho_o d}\int_0^\infty \frac{\mathrm{Im}\left(\Gamma_{p_k p_c}(\omega)\right)}{\omega} d\omega \\ &-\frac{\sin(\phi)}{3\rho_o d}\int_0^\infty \frac{\mathrm{Im}\left(\Gamma_{p_c p_m}(\omega)\right)}{\omega} d\omega \\ &-\frac{\sin(\phi)}{3\rho_o d}\int_0^\infty \frac{\mathrm{Im}\left(\Gamma_{p_c p_l}(\omega)\right)}{\omega} d\omega. \end{aligned} \tag{12}$$

The relations between the various pairs of microphone signals are given by

$$p_m(t) \approx \frac{1}{1 - \alpha(\omega)\kappa\tau_{m,c}} p_c(t + \tau_{m,c}), \tag{13}$$

$$p_l(t) \approx [1 - \alpha(\omega)\kappa\tau_{c,l}] p_c(t - \tau_{c,l}), \tag{14}$$

and

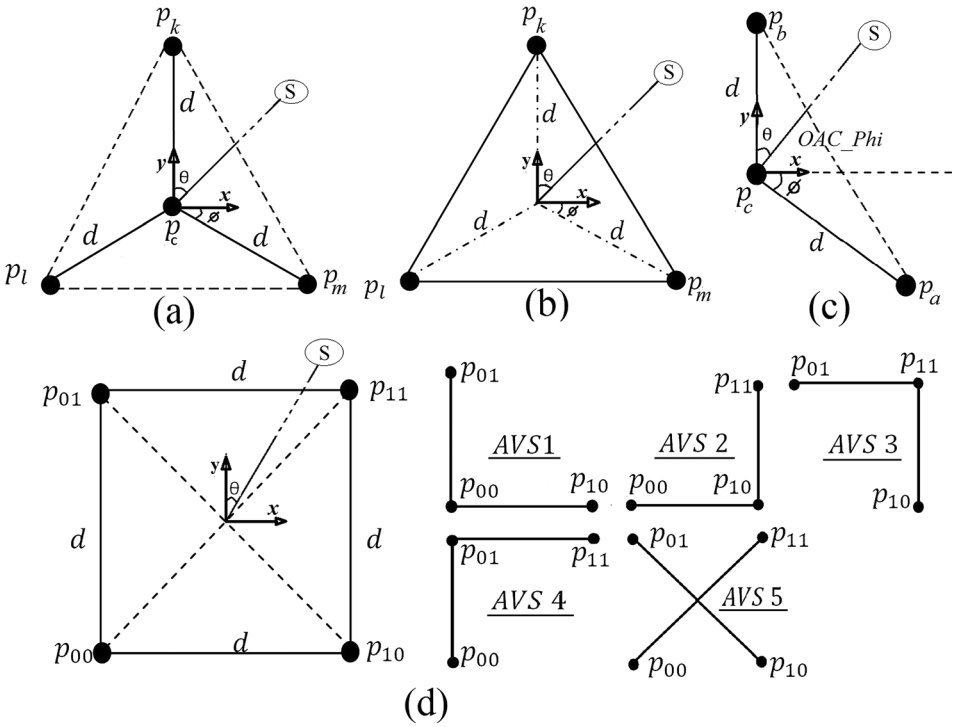

FIG. 2. Microphone configurations for AVS. Circles indicate omni-directional microphone, S indicates the sound source in the far-field. (a) Star configuration, having four measured signals, i.e., p_c, p_k, p_l, and p_m. (b) Delta configuration, having three measured signals, i.e., p_k, p_l, and p_m. (c) Three-microphone obtuse angle configuration with two pressure differences, having three measured signals, i.e., p_a, p_b, and p_c, (d) Square configuration (left) and its sub-configurations (right), having measured signals p_{00}, p_{10}, p_{11}, and p_{01}.

$$p_k(t) \approx \frac{1}{1-\alpha(\omega)\kappa\tau_{k,c}} p_c(t+\tau_{k,c}). \tag{15}$$

Using Eqs. (12) to (15), the intensity along the y-axis is expressed in terms of the PSD of $p_c(t)$ as

$$\begin{aligned} I_y^{\text{star}} = &\frac{1}{3\rho_o d}\int_0^\infty \frac{\Gamma_{p_c p_c}(\omega)\sin(\omega\tau_{k,c})}{[1-\kappa\tau_{k,c}\alpha(\omega)]\omega} d\omega \\ &+ \frac{\sin(\phi)}{3\rho_o d}\int_0^\infty \frac{\Gamma_{p_c p_c}(\omega)\sin(\omega\tau_{c,m})}{[1+\kappa\tau_{c,m}\alpha(\omega)]\omega} d\omega \\ &+ \frac{\sin(\phi)}{3\rho_o d}\int_0^\infty \frac{\Gamma_{p_c p_c}(\omega)\sin(\omega\tau_{c,l})}{[1+\kappa\tau_{c,l}\alpha(\omega)]\omega} d\omega. \end{aligned} \tag{16}$$

Similarly, the average intensity component along the x axis is given by

$$\begin{aligned} I_x^{\text{star}} = &\frac{\cos(\phi)}{3\rho_o d}\int_0^\infty \frac{\Gamma_{p_c p_c}(\omega)\sin(\omega\tau_{m,c})}{[1-\kappa\tau_{m,c}\alpha(\omega)]\omega} d\omega \\ &+ \frac{\cos(\phi)}{3\rho_o d}\int_0^\infty \frac{\Gamma_{p_c p_c}(\omega)\sin(\omega\tau_{c,l})}{[1+\kappa\tau_{c,l}\alpha(\omega)]\omega} d\omega. \end{aligned} \tag{17}$$

The DoA estimate is given by $\hat{\theta}^{\text{star}} = \tan^{-1}(I_x^{\text{star}}/I_y^{\text{star}})$, where I_x^{star} and I_y^{star} are obtained using Eqs. (16) and (17), respectively. If the measured signal $p_c(t)$ is sinusoidal, i.e., $p_c(t) = A\cos(\omega_o t + \phi_l)$, then the DoA estimate is given by

$$\hat{\theta}^{\text{star}}_{\text{sinusoidal source}} = \tan^{-1}\left[\frac{\dfrac{\sin(\omega_0\tau_{m,c})}{[1-\kappa\tau_{m,c}\alpha(\omega_0)]} + \dfrac{\sin(\omega_0\tau_{c,l})}{[1+\kappa\tau_{c,l}\alpha(\omega_0)]}}{\dfrac{\sec(\phi)\sin(\omega_0\tau_{k,c})}{[1-\kappa\tau_{k,c}\alpha(\omega_0)]} + \dfrac{\tan(\phi)\sin(\omega_0\tau_{c,m})}{[1+\kappa\tau_{c,m}\alpha(\omega_0)]} + \dfrac{\tan(\phi)\sin(\omega_0\tau_{c,l})}{[1+\kappa\tau_{c,l}\alpha(\omega_0)]}}\right], \tag{18}$$

where ω_o is the angular frequency of the sinusoidal signal.

B. Delta configuration

The delta configuration consists of three microphones as shown in Fig. 2(b). Let $p_k(t)$, $p_l(t)$, and $p_m(t)$ be the measured pressure signals at the three vertices of the delta configuration. There is no difference in geometrical structure between the star and delta configurations except the removal of the center microphone in the delta configuration. The difference is only in selecting cross power spectral density pairs. There are three pairs of microphones that give three intensity vector components aligned with the three solid lines. Using Eq. (7), the average intensity component for the delta configuration along the x axis is given by

$$\begin{aligned} I_x^{\text{delta}} = &-\frac{1}{3\sqrt{3}\rho_o d}\int_0^\infty \frac{\text{Im}\left(\Gamma_{p_m p_l}(\omega)\right)}{\omega} d\omega \\ &- \frac{\sin(\phi)}{3\sqrt{3}\rho_o d}\int_0^\infty \frac{\text{Im}\left(\Gamma_{p_m p_k}(\omega)\right)}{\omega} d\omega \\ &- \frac{\sin(\phi)}{3\sqrt{3}\rho_o d}\int_0^\infty \frac{\text{Im}\left(\Gamma_{p_k p_l}(\omega)\right)}{\omega} d\omega. \end{aligned} \tag{19}$$

The pressure waveform $p_l(t)$ is a delayed and attenuated version of $p_m(t)$, so the relation between $p_m(t)$ and $p_l(t)$ is given by

$$p_m(t) \approx \frac{1}{1-\alpha(\omega)\kappa\tau_{m,l}} p_l(t+\tau_{m,l}). \tag{20}$$

Similarly, the relation between $p_k(t)$ and $p_l(t)$ is given by

$$p_k(t) \approx \frac{1}{1-\alpha(\omega)\kappa\tau_{k,l}} p_l(t+\tau_{k,l}). \tag{21}$$

Using Eqs. (19) to (21), the intensity along the x axis is expressed in terms of the PSD of $p_l(t)$ as

$$I_x^{\text{delta}} = \frac{1}{3\sqrt{3}\rho_o d}\int_0^\infty \frac{\Gamma_{p_l p_l}(\omega)\sin(\omega\tau_{m,l})}{[1-\kappa\tau_{m,l}\alpha(\omega)]\omega} d\omega + \frac{\sin(\phi)}{3\sqrt{3}\rho_o d}\int_0^\infty \frac{\Gamma_{p_l p_l}(\omega)\sin\{\omega(\tau_{m,l}-\tau_{k,l})\}}{[1-\kappa\tau_{m,l}\alpha(\omega)][1-\kappa\tau_{k,l}\alpha(\omega)]\omega} d\omega + \frac{\sin(\phi)}{3\sqrt{3}\rho_o d}\int_0^\infty \frac{\Gamma_{p_l p_l}(\omega)\sin(\omega\tau_{k,l})}{[1-\kappa\tau_{k,l}\alpha(\omega)]\omega} d\omega. \tag{22}$$

The average intensity component along the y-axis is similarly given by

$$I_y^{\text{delta}} = \frac{\cos(\phi)}{3\sqrt{3}\rho_o d}\int_0^\infty \frac{\Gamma_{p_l p_l}(\omega)\sin\{\omega(\tau_{k,l}-\tau_{m,l})\}}{[1-\kappa\tau_{k,l}\alpha(\omega)][1-\kappa\tau_{m,l}\alpha(\omega)]\omega} d\omega + \frac{\cos(\phi)}{3\sqrt{3}\rho_o d}\int_0^\infty \frac{\Gamma_{p_l p_l}(\omega)\sin(\omega\tau_{k,l})}{[1-\kappa\tau_{k,l}\alpha(\omega)]\omega} d\omega. \tag{23}$$

The DoA estimate is given by $\hat{\theta}^{\text{delta}} = \tan^{-1}(I_x^{\text{delta}}/I_y^{\text{delta}})$, where I_x^{delta} and I_y^{delta} are obtained using Eqs. (22) and (23), respectively. For the sinusoidal source of frequency ω_o, the DoA estimate is given by

$$\hat{\theta}^{\text{delta}}_{\text{sinusoidal source}} = \tan^{-1}\left[\frac{\frac{\sin(\omega_0\tau_{m,l})[1-\kappa\tau_{k,l}\alpha(\omega_0)]}{\cos(\phi)[1-\kappa\tau_{m,l}\alpha(\omega_0)]} + \tan(\phi)\left\{\sin(\omega_0\tau_{k,l}) - \frac{\sin\{\omega_0(\tau_{k,l}-\tau_{m,l})\}}{[1-\kappa\tau_{m,l}\alpha(\omega_0)]}\right\}}{\frac{\sin\{\omega_0(\tau_{k,l}-\tau_{m,l})\}}{[1-\kappa\tau_{m,l}\alpha(\omega_0)]} + \sin(\omega_0\tau_{k,l})}\right]. \tag{24}$$

The analytical results of delta and star configurations for a 1 kHz source signal at various DoA is given in Table I. It can be observed that the star configuration and delta configuration have nearly identical performance and the possible source of error in the analytical results is due to approximation of the pressure-gradient and pressure at the midpoint of two closely spaced microphones.

C. Obtuse angle configuration

The three-microphone obtuse angle configuration is shown in Fig. 2(c). In this configuration, two intensity vectors are formed aligned with the solid lines. The angle between the lines joining the two pairs of microphones is $90^\circ+\phi$ and let the respective configuration be called OACϕ. Let $p_a(t)$, $p_b(t)$, and $p_c(t)$ be the measured pressure signal by the three microphones of this configuration. This AVS configuration is same as the star configuration except for the removal of one microphone from the third quadrant and $\phi = 30^\circ$. The intensity components along the y-axis and x axis are expressed in terms of PSD of $p_c(t)$ as

$$I_y^{OAC\phi} = \frac{\sin(\phi)}{2\rho_o d}\int_0^\infty \frac{\Gamma_{p_c p_c}(\omega)}{\omega}\frac{\sin(\omega\tau_{ac})}{[1-\kappa\tau_{ac}\alpha(\omega)]} d\omega + \frac{1}{2\rho_o d}\int_0^\infty \frac{\Gamma_{p_c p_c}(\omega)}{\omega}\frac{\sin(\omega\tau_{bc})}{[1-\kappa\tau_{bc}\alpha(\omega)]} d\omega \tag{25}$$

and

$$I_x^{OAC\phi} = \frac{\cos(\phi)}{2\rho_o d}\int_0^\infty \frac{\Gamma_{p_c p_c}(\omega)\sin(\omega\tau_{ac})}{[1-\kappa\tau_{ac}\alpha(\omega)]\omega} d\omega, \tag{26}$$

where $\Gamma_{p_c p_c}(\omega)$ is the PSD of $p_c(t)$.

D. Square configuration

The square configuration consists of four microphones which can be seen as a superset of five different sub-configurations as shown in Fig. 2(d). Each sub-configuration uses two pairs of microphone signals to estimate the two orthogonal intensity components. Further, some new AVS configurations can be created by using two or more of these sub-configurations; like AVS13 that uses the average of the DoA estimates of AVS1 and AVS3; and AVS1234 which is an average of the DoA estimates of AVS1, AVS2, AVS3, and AVS4.

TABLE I. The analytical results of delta and star configurations for 1 kHz source signal at various DoA with $d = 10$ mm.

	Analytical results, DoA (degrees)	
Actual DoA (degrees)	Delta configuration	Star configuration
(0, 90, 180, 270)	(0.000, 90.291, 180.000, 269.713)	(0.000, 90.287, 179.999, 269.714)
(15, 105, 195, 285)	(14.795, 105.204, 195.203, 284.796)	(14.798, 105.202, 195.202, 284.797)
(30, 120, 210, 300)	(29.708, 120, 210.286, 300.000)	(29.712, 120.000, 210.285, 300.000)
(45, 135, 225, 315)	(44.792, 134.796, 225.201, 315.204)	(44.795, 134.798, 225.201, 315.203)
(60, 150, 240, 330)	(60.000, 149.711, 240.000, 330.288)	(60.000, 149.7135, 240.000, 330.286)
(75, 165, 255, 345)	(75.207, 164.795, 254.798, 345.203)	(75.204, 164.796, 254.799, 345.201)

TABLE II. DoA estimate for several AVS configurations in terms of time delay of arrival $\tau_{i,j}$ between the ith and jth microphones and θ is the actual angle of arrival.

DoA estimate	Expressions
$\hat{\theta}_{\text{delta}}$	$\tan^{-1}\left[\dfrac{\int_0^\infty \dfrac{\Gamma_{p_i p_l}(\omega)}{\omega}\left[\dfrac{\sin(\omega\tau_{m,l})}{[1-\kappa\tau_{m,l}\alpha(\omega)]}+\dfrac{\sin(\phi)}{1-\kappa\tau_{k,l}\alpha(\omega)}\left\{\dfrac{\sin\{\omega(\tau_{m,l}-\tau_{k,l})\}}{[1-\kappa\tau_{m,l}\alpha(\omega)]}+\sin(\omega\tau_{k,l})\right\}\right]d\omega}{\cos(\phi)\int_0^\infty \dfrac{\Gamma_{p_i p_l}(\omega)}{[1-\kappa\tau_{k,l}\alpha(\omega)]\omega}\left[\dfrac{\sin\{\omega(\tau_{k,l}-\tau_{m,l})\}}{[1-\kappa\tau_{m,l}\alpha(\omega)]}+\sin(\omega\tau_{k,l})\right]d\omega}\right]$
$\hat{\theta}_{\text{star}}$	$\tan^{-1}\left[\dfrac{\cos(\phi)\int_0^\infty \dfrac{\Gamma_{p_c p_c}(\omega)}{\omega}\left[\dfrac{\sin(\omega\tau_{m,c})}{[1-\kappa\tau_{m,c}\alpha(\omega)]}+\dfrac{\sin(\omega\tau_{c,l})}{[1+\kappa\tau_{c,l}\alpha(\omega)]}\right]d\omega}{\int_0^\infty \dfrac{\Gamma p_c p_c(\omega)}{\omega}\left[\dfrac{\sin(\omega\tau_{k,c})}{[1-\kappa\tau_{k,c}\alpha(\omega)]}+\sin(\phi)\left\{\dfrac{\sin(\omega\tau_{c,m})}{[1+\kappa\tau_{c,m}\alpha(\omega)]}+\dfrac{\sin(\omega\tau_{c,l})}{[1+\kappa\tau_{c,l}\alpha(\omega)]}\right\}\right]d\omega}\right]$
$\hat{\theta}_{\text{AVS1}}$	$\tan^{-1}\left[\dfrac{\int_0^\infty \dfrac{\Gamma_{p_{00}p_{00}}(\omega)\sin(\omega\tau_{10,00})}{[1-\kappa\tau_{10,00}\alpha(\omega)]\omega}d\omega}{\int_0^\infty \dfrac{\Gamma_{p_{00}p_{00}}(\omega)\sin(\omega\tau_{01,00})}{[1-\kappa\tau_{01,00}\alpha(\omega)]\omega}d\omega}\right]$
$\hat{\theta}_{\text{AVS2}}$	$\tan^{-1}\left[\dfrac{\int_0^\infty \dfrac{\Gamma_{p_{00}p_{00}}(\omega)\sin(\omega\tau_{10,00})}{\omega}d\omega}{\int_0^\infty \dfrac{\Gamma_{p_{00}p_{00}}(\omega)\sin\{\omega(\tau_{10,00}-\tau_{11,00})\}}{[1-\kappa\tau_{11,00}\alpha(\omega)]\omega}d\omega}\right]$
$\hat{\theta}_{\text{AVS3}}$	$\tan^{-1}\left[\dfrac{\int_0^\infty \dfrac{\Gamma_{p_{00}p_{00}}(\omega)\sin\{\omega(\tau_{11,00}-\tau_{01,00})\}}{[1-\kappa\tau_{01,00}\alpha(\omega)]\omega}d\omega}{\int_0^\infty \dfrac{\Gamma_{p_{00}p_{00}}(\omega)\sin\{\omega(\tau_{11,00}-\tau_{10,00})\}}{[1-\kappa\tau_{10,00}\alpha(\omega)]\omega}d\omega}\right]$
$\hat{\theta}_{\text{AVS4}}$	$\tan^{-1}\left[\dfrac{\int_0^\infty \dfrac{\Gamma_{p_{00}p_{00}}(\omega)\sin\{\omega(\tau_{01,00}-\tau_{11,00})\}}{[1-\kappa\tau_{11,00}\alpha(\omega)][1-\kappa\tau_{01,00}\alpha(\omega)]\omega}d\omega}{\int_0^\infty \dfrac{\Gamma_{p_{00}p_{00}}(\omega)\sin(\omega\tau_{01,00})}{[1-\kappa\tau_{01,00}\alpha(\omega)]\omega}d\omega}\right]$
$\hat{\theta}_{\text{AVS5}}$	$-45^\circ+\tan^{-1}\left[\dfrac{-\int_0^\infty \dfrac{\Gamma_{p_{00}p_{00}}(\omega)\sin(\tau_{11,00})}{[1-\kappa\tau_{11,00}\alpha(\omega)]\omega}d\omega}{\int_0^\infty \dfrac{\Gamma_{p_{00}p_{00}}(\omega)\sin\{\omega(\tau_{10,00}-\tau_{01,00})\}}{[1-\kappa\tau_{10,00}\alpha(\omega)][1-\kappa\tau_{01,00}\alpha(\omega)]\omega}d\omega}\right]$

Expressions for time delay of arrival

$\tau_{m,l}=\dfrac{2d\cos\phi\sin\theta}{\kappa}$	$\tau_{k,l}=\dfrac{2d\cos\phi\cos\left(\frac{\pi}{6}-\theta\right)}{\kappa}$	$\tau_{m,c}=\dfrac{d\sin\left(\theta-\frac{\pi}{6}\right)}{\kappa}$	$\tau_{c,l}=\dfrac{d\cos\left(\theta-\frac{\pi}{3}\right)}{\kappa}$
$\tau_{k,c}=\dfrac{d\cos\theta}{\kappa}$	$\tau_{10,00}=\dfrac{d\sin\theta}{\kappa}$	$\tau_{01,00}=\dfrac{d\cos\theta}{\kappa}$	$\tau_{11,00}=\dfrac{\sqrt{2}d\cos(45^\circ-\theta)}{\kappa}$

TABLE III. Simulation setup specifications.

Specifications/Variable	Values/type
Speed of sound (m/s), κ	343
Azimuth (deg.), θ	0, 15,…, 345
Source range (m), r	1
Signal durations (ms)	25, 100, 500, and 1000
Source signal type	Sinusoidal (1 kHz)
Sampling rates (kHz), F_s	48
SNR (dB)	∞, 30, 26,…, 10
Noise type	Additive White Gaussian noise
Number of realizations	10 000
Microphone diameter (mm)	0 and 3.3
Microphone separation (mm), d	1, 5, 10, 15, …, 60
Attenuation factor (1/m), α	0.989 (at 1 kHz)

Let $p_{00}(t)$, $p_{10}(t)$, $p_{11}(t)$, and $p_{01}(t)$ denote the measured pressure signals at the four vertices of the square configuration. For AVS1, the intensity along the x axis is expressed in terms of the PSD of $p_{00}(t)$ as

$$I_x^{\mathrm{AVS1}} = \frac{1}{2\rho_o d}\int_0^{\infty} \frac{\Gamma_{p_{00}p_{00}}(\omega)\sin(\omega\tau_{10,00})}{[1-\kappa\tau_{10,00}\alpha(\omega)]\omega}d\omega, \tag{27}$$

where $\Gamma_{p_{00}p_{00}}(\omega)$ is the PSD of $p_{00}(t)$. Similarly, the intensity along the y-axis is given by

$$I_y^{\mathrm{AVS1}} = \frac{1}{2\rho_o d}\int_0^{\infty} \frac{\Gamma_{p_{00}p_{00}}(\omega)\sin(\omega\tau_{01,00})}{[1-\kappa\tau_{01,00}\alpha(\omega)]\omega}d\omega. \tag{28}$$

Likewise, the intensity components using all the five subconfigurations AVS1, AVS2, AVS3, AVS4, and AVS5 are calculated and their DoA estimates in terms of time delay of arrival $\tau_{i,j}$ between the ith and jth microphones are listed in Table II. The time delay of arrival expressions are also given in this table and it is a function of the actual DoAs. The relation between the estimated angle using AVS1, AVS2, AVS3, and AVS4 are given as $\hat{\theta}_{\mathrm{AVS2}} = 270^\circ + \hat{\theta}_{\mathrm{AVS1}}$, $\hat{\theta}_{\mathrm{AVS3}} = 180^\circ + \hat{\theta}_{\mathrm{AVS1}}$, and $\hat{\theta}_{\mathrm{AVS4}} = 90^\circ + \hat{\theta}_{\mathrm{AVS1}}$. For example, from the AVS geometry it can be verified that results of the first quadrant for AVS1 will be valid for (a) the second quadrant for AVS2, (b) the third quadrant for AVS3, and (c) the fourth quadrant for AVS4.

V. SIMULATION SETUP AND RESULTS

A. Simulation setup

The numerical simulation for DoA estimation in 2-D has been done for the AVS configurations presented in Sec. IV. An acoustic signal in air emitted by an omni-directional point source has been generated and recorded by the AVS sensors using Finite Element Method tool, viz., COMSOL Multiphysics version 4.4 and the simulation setup specifications are given in Table III. In this section zero-size microphones are considered and non-zero size microphone simulation results are used for comparison with experimental results in Sec. VI. The performance evaluation has been illustrated in terms of angular error (AE), absolute angular error (AAE) and root-mean-square angular error (RMSAE) that are defined in Eqs. (29) to (31). The AE for a particular angular location of the radiating source can be expressed as

$$\mathrm{AE} = \frac{1}{N}\sum_{i=1}^{N} \cos^{-1}\left(\mathbf{u}^{\mathbf{T}}\hat{\mathbf{u}}_{\mathbf{i}}\right), \tag{29}$$

where $\mathbf{u}$ is the unit vector pointing to the sound source, $\hat{\mathbf{u}}_{\mathbf{i}}$ is its estimate at the ith realization, $(*)^T$ indicates transpose, and N is the total number of independent realizations considering additive noise. The AAE is given by

$$\mathrm{AAE} = \frac{1}{N}\left|\sum_{i=1}^{N} \cos^{-1}\left(\mathbf{u}^{\mathbf{T}}\hat{\mathbf{u}}_{\mathbf{i}}\right)\right|. \tag{30}$$

The RMSAE is defined as

$$\mathrm{RMSAE} = \sqrt{\frac{\sum_{i=1}^{N}\left\{\cos^{-1}\left(\mathbf{u}^{\mathbf{T}}\hat{\mathbf{u}}_{\mathbf{i}}\right)\right\}^2}{N}}. \tag{31}$$

Wherever AAE and RMSAE are averaged over all the different angular source locations, the symbols $\overline{\mathrm{AAE}}$ and $\overline{\mathrm{RMSAE}}$ are used. These are defined, respectively, as

$$\overline{\mathrm{AAE}}_{15k_1:15k_2} = \frac{1}{k_2-k_1+1}\sum_{k=k_1}^{k_2}\mathrm{AAE}(15k), \tag{32}$$

$$\overline{\mathrm{RMSAE}}_{15k_1:15k_2} = \frac{1}{k_2-k_1+1}\sum_{k=k_1}^{k_2}\mathrm{RMSAE}(15k), \tag{33}$$

where the argument $15k$ represents the direction of the source in degrees and subscripts $15k_1$:$15k_2$ give the range of angles used for averaging over the different angular locations of the source with an increment of 15°, and encompassing all four quadrants. All the error results are presented after removal of 10% outliers of the 10000 independent realizations for the case when noise is present. The performance has been compared for the different AVS microphone configurations and also with some other standard microphone-array based DoA methods, i.e., MUSIC and GCC.[39–41] This simulation study also encompasses the effects of varying the separation d between the microphones of the corresponding AVSs and varying the sinusoidal signal duration of a source which emits 1 kHz signal in the absence of noise.

B. Simulation results

1. Tonal source with varying durations

In this section, sinusoidal source signals of different durations are simulated for DoA estimation in the absence of noise with $d = 10$ mm. Figure 3 show the AE for the sinusoidal source of 1 kHz of durations 25, 100, 500, and 1000 ms sampled at 48 kHz and located at a range of 1 m from the center of the AVSs. It is observed that increasing the sinusoidal signal duration from 25 to 1000 ms does not affect the

AE performance of the different AVS configurations. Also, the estimated DoA is not subject to left-right ambiguity as the sign of the orthogonal intensity components can indicate the source quadrant that is able to resolve the source direction in all the four quadrants.

The absolute of AE for the star and delta configurations are less than 0.005° for the DoAs 0°, 60°, 120°, 180°, 240°, and 300°. These DoAs lie on the axis of symmetry of the AVS (line joining the source and the center of the AVS configuration), where the error in DoA estimate due to the pressure-gradient approximation is not present. Similarly for the other sub-configurations formed using square configurations, the absolute of AE are less than 0.01° at the DoAs when the source lies on the axis of symmetry of the AVS configuration. The star and delta configurations offer almost identical AE performance. Table IV gives the values of $\overline{\text{AAE}}_{0°:120°}$, $\overline{\text{AAE}}_{120°:240°}$, and $\overline{\text{AAE}}_{240°:360°}$ which are approximately equal across the three different sectors. It indicates that the star and the delta configurations give similar average performance across the azimuth intervals [0°–120°], [120°–240°], and [240°–360°] which is due to symmetric nature of star and delta configurations in these

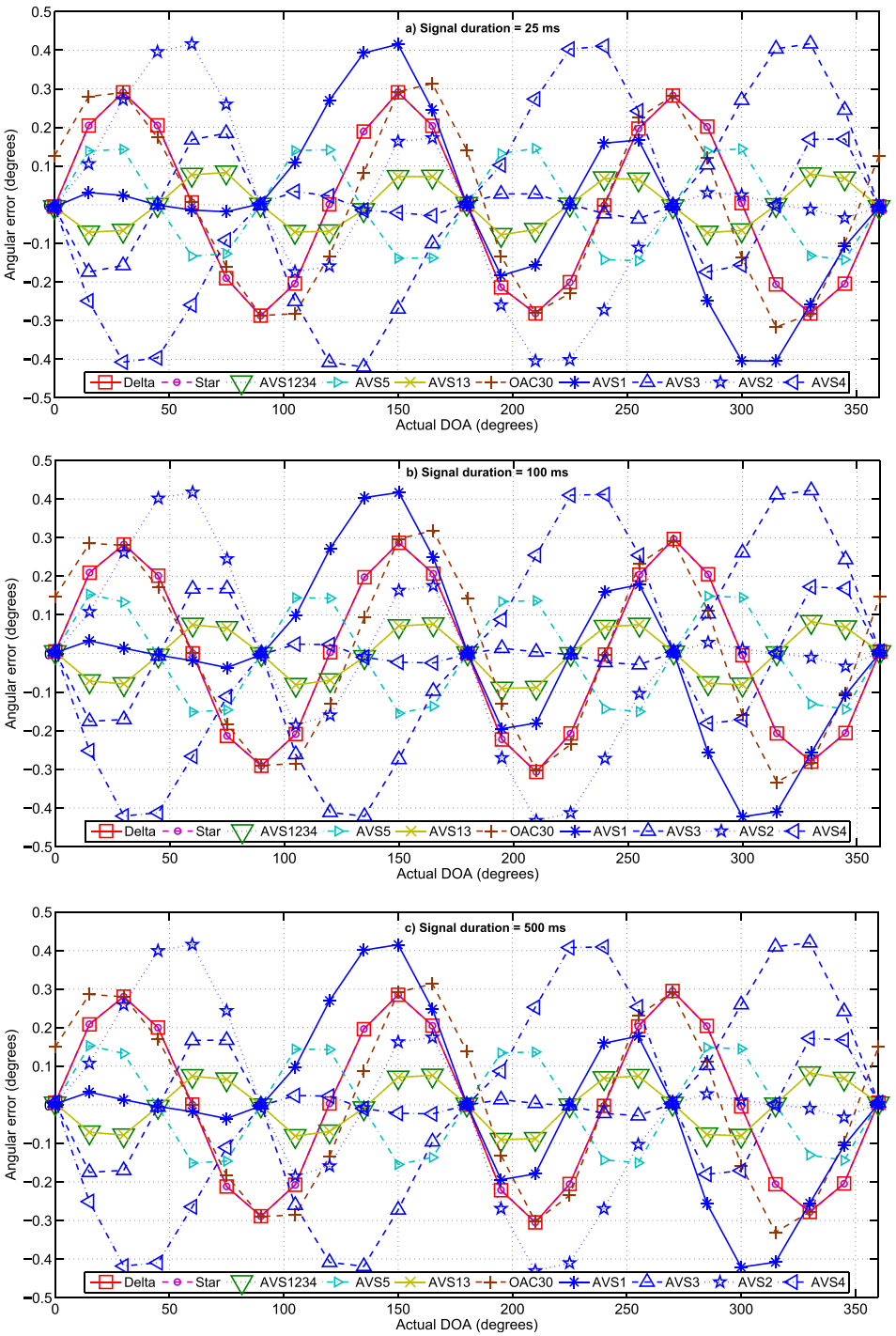

FIG. 3. (Color online) AE versus DoAs for several AVS configurations for sinusoidal source of 1 kHz without additive noise located at a range of 1 m with $d = 10$ mm and received signals of durations (a) 25 ms, (b) 100 ms, (c) 500 ms, and (d) 1000 ms.

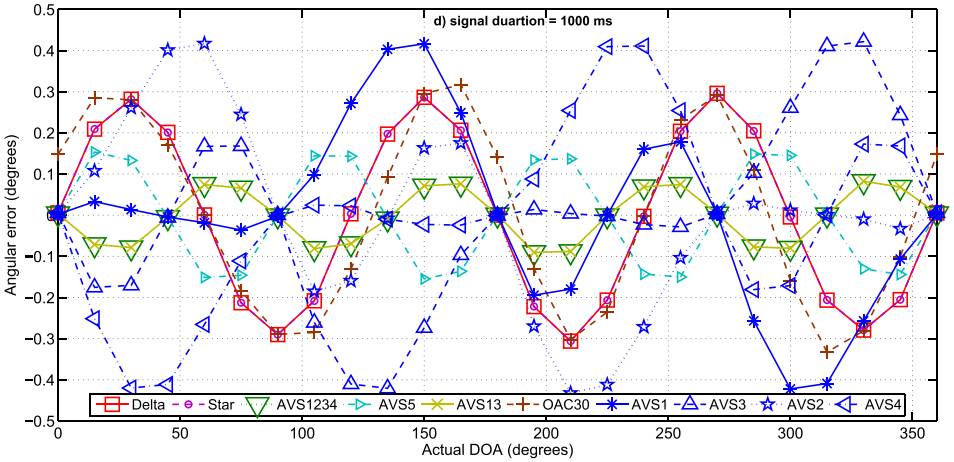

FIG. 3. (Color online) (*Continued*)

DoAs intervals. The geometrical placement of microphones in the delta configuration is the same as the star configuration except for the removal of center microphone. In terms of computation, both configurations need to calculate the three CPSDs, but the delta configuration requires one less microphone than the star configuration. Therefore, the delta configuration may be preferred over the star configuration for the no noise case; however, we also see in Sec. V B 3 that this conclusion is also valid if uncorrelated noise is also present, down to 10 dB.

The absolute of AE for OAC30 is less than 0.005° at 60° and 240° DoAs which lies on the axis of symmetry of the configuration and the error in DoA estimate due to the pressure-gradient approximation is not present. The $\overline{\text{AAE}}$ performance is the same across the azimuth intervals [120°–240°] and [300°–240°]. In contrast to the delta and the star configurations, the AE for OAC30 configuration are non-zero for the source location at 0°, 120°, 180° and 300°. This is due to the asymmetric structure of the OAC30 along the line joining the sources and the origin which does not allow elimination of the effect due to the pressure-gradient error. These observations can be verified by plotting the errors obtained by the expressions derived in Sec. IV.

From Fig. 3 and Table V, it can be observed that among the four quadrants the AE and $\overline{\text{AAE}}$ are minimum in the first quadrant for AVS1, second quadrant for AVS2, third quadrant for AVS3, and fourth quadrant for AVS4. It can be concluded that the error is minimum in the quadrant in which the AVS is oriented, however the $\overline{\text{AAE}}_{0°:345°}$ over all the four quadrants is the same for all the four AVSs. The $\overline{\text{AAE}}$ performance for AVS13, AVS1234, and AVS5 is uniform across all the four quadrants because it has axes of symmetry which passes from all the four quadrants. Among these three AVS configurations, AVS13 and AVS1234 give lower $\overline{\text{AAE}}_{0°:345°}$ than AVS5. This is due to the larger separation of microphones, i.e., $\sqrt{2}d$ while calculating pressure-gradient in case of AVS5 compared to AVS13 and AVS1234. However, AVS13 and AVS1234 need to compute four CPSDs compared to two CPSDs in the case of AVS5. The $\overline{\text{AAE}}_{0°:345°}$ for the AVS13, AVS1234, and AVS5 are lower compared to AVS1, AVS2, AVS3, and AVS4. If the quadrant in which the source lies is known, then accordingly AVS1, AVS2, AVS3, and AVS4 may be used because these configurations give lower AE in one of the four quadrants. However. if the quadrant is not known then a two step process can be followed, i.e., first determine the quadrant using any AVS configuration and then find the DoA using the appropriate configuration amongst AVS1, AVS2, AVS3, and AVS4. As shown in Fig. 3, the maximum AE across the four quadrants for (a) AVS1, AVS2, AVS3 and AVS4 is 0.41°, (b) delta and star configurations is 0.29°, (c) AVS5 is 0.14°, and (d) AVS13 and AVS1234 is 0.07°. Among all the AVS configurations, the minimum $\overline{\text{AAE}}_{0°:345°}$ over all the four quadrants is achieved for AVS13 and AVS1234 and its value is 0.048° as it uses four CPSD computations and have more axes of symmetry for the angular range from 0° to 360°.

TABLE IV. $\overline{\text{AAE}}$ (degrees) for star, delta and OAC30 AVS configurations ($d = 10$ mm) for different quadrant for sinusoidal source of 1 kHz at a range of 1 m.

	$\overline{\text{AAE}}$ (degrees)		
	$\overline{\text{AAE}}_{0°:120°}$	$\overline{\text{AAE}}_{120°:240°}$	$\overline{\text{AAE}}_{240°:360°}$
Star	0.154	0.153	0.153
Delta	0.154	0.153	0.153
OAC30	0.193	0.178	0.176

2. Tonal source with varying microphone separation

The separation d between the microphones of the AVSs given in Fig. 2 are varied from 1 to 60 mm for a sinusoidal source of 1 kHz and 25 ms duration at a range of 1 m. Figure 4 shows the FEM simulation and analytical results of $\overline{\text{AAE}}_{0°:345°}$ across the four quadrants for the different values of d. These performance results show that on increasing the microphone separation, $\overline{\text{AAE}}_{0°:345°}$ increases for all the AVS configurations. This is due to the increase in error in the pressure-gradient approximation using the FD method [see Fig. 1, Eqs. (1) and (2)] and also due to the error in approximating the pressure at the mid-point of the line joining the two microphones. It is also observed that $\overline{\text{AAE}}_{0°:345°}$ is lowest for AVS13 and AVS1234 than the other AVS configurations for $1 \leq d \leq 35$ mm, this is due to cancellation of errors

TABLE V. $\overline{AAE}$ (degrees) for AVS1-5, AVS13 and AVS1234 ($d = 10$ mm) for the four quadrants for sinusoidal source of 1 kHz at a range of 1 m.

	$\overline{AAE}$ (degrees) for four Quadrants (Q1, Q2, Q3, and Q4)			
	$\overline{AAE}_{0^\circ:90^\circ}$ (Q1)	$\overline{AAE}_{270^\circ:360^\circ}$ (Q2)	$\overline{AAE}_{180^\circ:270^\circ}$ (Q3)	$\overline{AAE}_{90^\circ:180^\circ}$ (Q4)
AVS1	0.013	0.204	0.096	0.205
AVS2	0.208	0.015	0.207	0.097
AVS3	0.098	0.206	0.017	0.207
AVS4	0.201	0.097	0.205	0.017
AVS5	0.078	0.082	0.081	0.081
AVS13	0.043	0.043	0.040	0.042
AVS1234	0.043	0.042	0.040	0.042

of opposite signs, i.e., the signs of AE for AVS1 and AVS2 are opposite to the signs of AE for AVS3 and AVS4, respectively, as given in Fig. 3. However, for $35 < d \leq 60$ mm, the $\overline{AAE}_{0^\circ:345^\circ}$ for delta and star configurations is smallest amongst all other AVS configurations considered in this paper and is equal to 1.225° at $d = 60$ mm whereas for AVS13 and AVS1234 it is equal to 1.871°. The delta and star configurations require only three CPSDs computations whereas AVS13 and AVS1234 configurations require four CPSDs computations. We can conclude that delta and star configurations are more robust against the error introduced by pressure-gradient and mid-point pressure approximation for larger microphone separations for ideal zero-size microphones. This is an added advantage for the practical consideration when microphone diameter is higher. For a practical point of view, the existing microphones that are of 3.3 mm diameter restrict the minimum separation between the centers of the microphones to be greater than 3.3 mm. But, if the microphones are very close to each other, the pressure difference between the microphone signals will be very small for low frequencies and for higher frequencies effects such as reflections from the microphone body, shadowing and diffraction will become important.

3. Performance evaluation in the presence of noise

The following simulation specifications have been used for the performance evaluation in this sub-section. The sound source is located at a range of 1 m with varying azimuth from 0° to 360° and emits a sinusoidal signal of 1 kHz of 25 ms duration. The signal is recorded by an AVS with microphone separation of 10 mm for different SNR values at the microphones. In these simulations, noise is considered with the assumption that it is uncorrelated across the

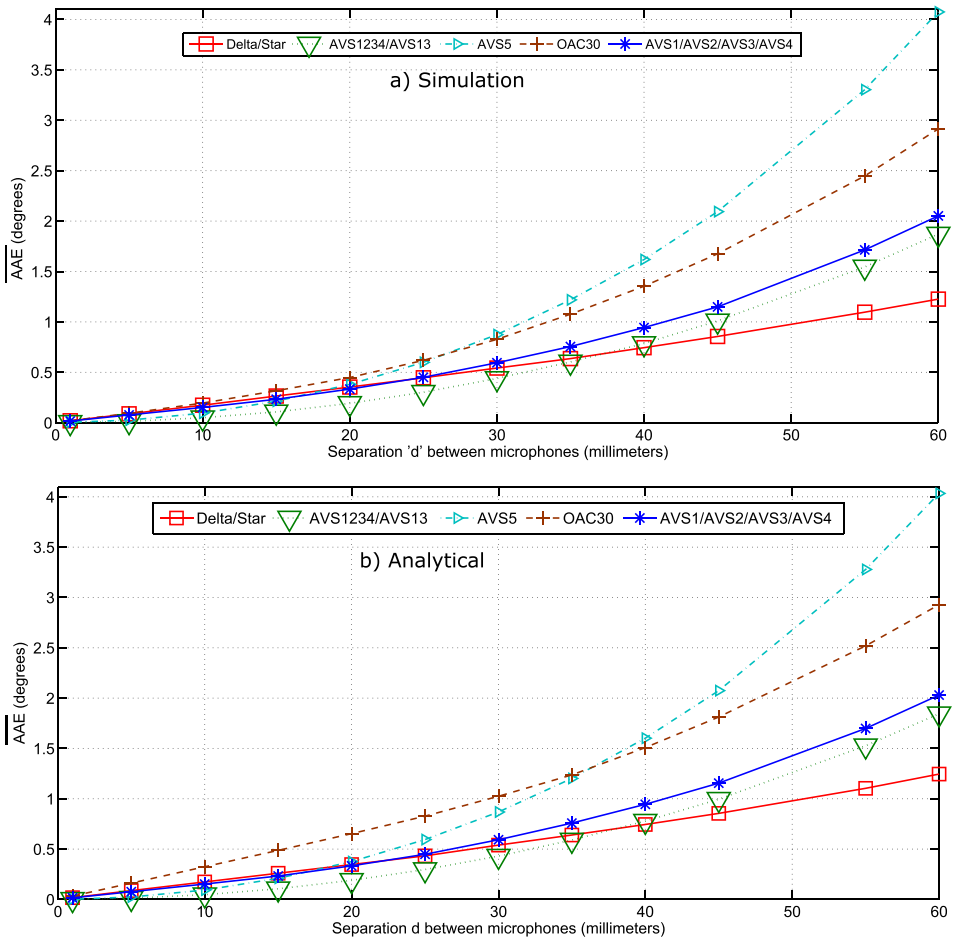

FIG. 4. (Color online) $\overline{AAE}_{0^\circ:345^\circ}$ versus microphone separation d for different AVS configurations for sinusoidal source of 1 kHz and 25 ms duration at a range of 1 m and there is no additive noise, (a) FEM simulation results and (b) analytical results.

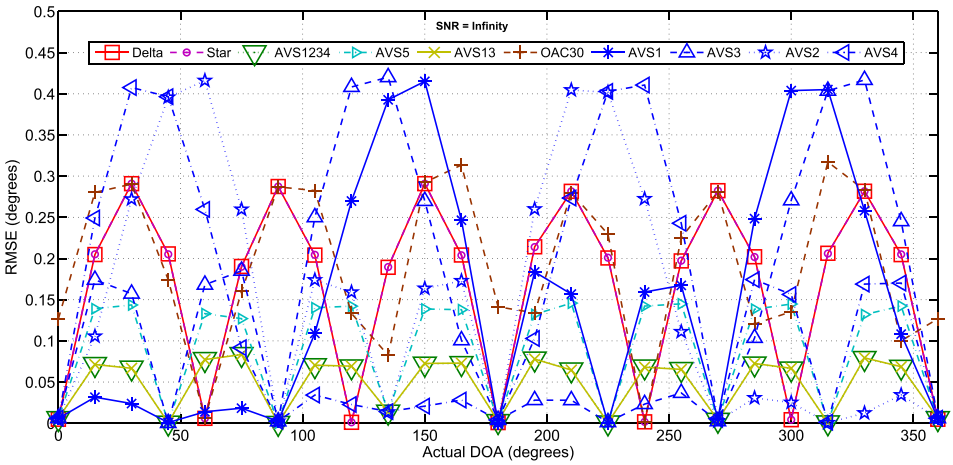

FIG. 5. (Color online) RMSAE versus DoAs for different AVS configurations when sound source is at a range of 1 m and emits 1 kHz sinusoidal signal of 25 ms duration, and there is no additive noise.

channels. The noise waveforms at the microphones of each AVS configuration are generated 10 000 times for each SNR and each angular location independently. The performance of different AVS configurations in the presence of noise is represented in terms of RMSAE, as it contains both bias as well as variance of the estimated DoAs. Figures 5 and 6 show the variation in RMSAE with DoA ranging from 0° to 360° for SNR values of ∞, 30, 26, 22, 18, 14, and 10 dB, respectively, and Table VI gives the $\overline{\text{RMSAE}}_{0°:345°}$ over all four quadrants. For the case when SNR is infinity, RMSAE contains only the absolute of bias error, but when SNR decreases, the standard deviation is found to be higher than the bias. At SNR = 30 dB, AVS13 and AVS1234 give the smallest value of $\overline{\text{RMSAE}}_{0°:345°}$. Also $\overline{\text{RMSAE}}_{0°:345°}$ for AVS5 is comparable to AVS13 and AVS1234 for SNR lower than 22 dB. The RMSAE for all DoAs are close to 2° for the delta and star configurations which is lowest amongst all AVS configurations at 10 dB SNR. The rate of increase in $\overline{\text{RMSAE}}_{0°:345°}$ with respect to decrease in SNR for the delta and star configurations are the lowest, so delta or star configuration may be the best choice amongst all the AVS configurations for SNR below 22 dB. This is due to more number of intensity components and their averaging, which will reduce the effect of noise. The performance of the delta and star AVS microphone configuration is almost identical for the different SNR values. This shows that even in the presence of noise, delta configuration should be preferred over the star configuration as it requires one less microphone.

4. Comparison of performance of AVS microphone configurations with GCC and MUSIC algorithms

The P-P based AVS microphone configurations have been studied as 2-D microphone-arrays of the same dimensions and compared. The DoA estimation methods like GCC and MUSIC have been applied for the microphone arrays and compared with acoustic intensity based DoA estimation for the AVS configurations. The GCC calculates the DoA based on the TDoA of the signals received at the spatially distributed microphones. For a pair of microphones and a sound source in the far field, the TDoA and DoA are related as

$$T_{12} \cong \frac{d \sin\theta}{\kappa}, \tag{34}$$

where T_{12} is the TDoA between the two microphones and θ is the DoA with respect to the normal of the line joining the two microphones. The estimated TDoA for a pair of microphones is obtained using the cross-correlation between the two received signals and is given by

$$T_{12} = \text{argmax} abs[R(l)], \tag{35}$$

where $R(l)$ is the cross-correlation function between the signals received at the two microphones. This method provides relatively poor estimation accuracy when sound source is located at the end-fire direction. As the separation between the microphones decreases the TDoA accuracy reduces for a given sampling rate. The GCC method also creates front-back ambiguity which can be removed using a third microphone. See, for example, Refs. 39 and 40 for a discussion on GCC. The MUSIC algorithm is based on decomposition of the covariance matrix of the recorded microphone signals in an array. The signal and noise sub-spaces are used to form a pseudo-spectrum function whose peak gives the estimated DoA of the sound source.[41] This method provides good angular resolution only at high SNR. Both GCC and MUSIC require search for the peak in the cross-correlation and pseudo-spectrum function, respectively. The intensity based DoA estimation accuracy can be significantly affected due to the directive interference or the presence of multiple sources.

The GCC and MUSIC methods are applied on the delta and square configurations with $d = 10$ mm and the sound source emits a 1 kHz sinusoidal signal at a range of 1 m. For the GCC method, if n ($n > 2$) microphones are present, then $n(n-1)/2$ number of estimates of TDoAs and DoAs are available for an angular location of a sound source; in the present simulation the TDoA that gives the minimum $\overline{\text{RMSAE}}$ is used for comparison with AVS. The received signals are interpolated by a factor of 100 before applying GCC to improve the accuracy of the TDoA estimate. In MUSIC, the peak of the pseudo-spectrum function is searched with an angular resolution of 0.1°. The results are given in Table VII, from which it can be inferred that at SNR of 18 dB and

above, the MUSIC algorithm for delta array configuration is comparable to the AVS based method, while GCC gives higher error due to its dependence on time resolution. At SNR below 18 dB the DoA estimation method based on the intensity vector gives lower error than the microphone-array based DoA estimation methods for the given microphone configurations. For the three-microphone delta configuration, at 10 dB SNR the improvement in $\overline{\text{RMSAE}}$ of the intensity vector based method is 38.20% and 74.72% over the MUSIC and the GCC methods, respectively. For the four-microphone square configuration, i.e., AVS5, at 10 dB SNR the improvement in the $\overline{\text{RMSAE}}$ using the intensity vector based method is 72.58% and 73.84% over the MUSIC and the GCC, respectively. It has been observed that in the presence of additive noise, DoA estimation improves when using the intensity based method with AVS compared to microphone-array based methods for the given microphone configurations.

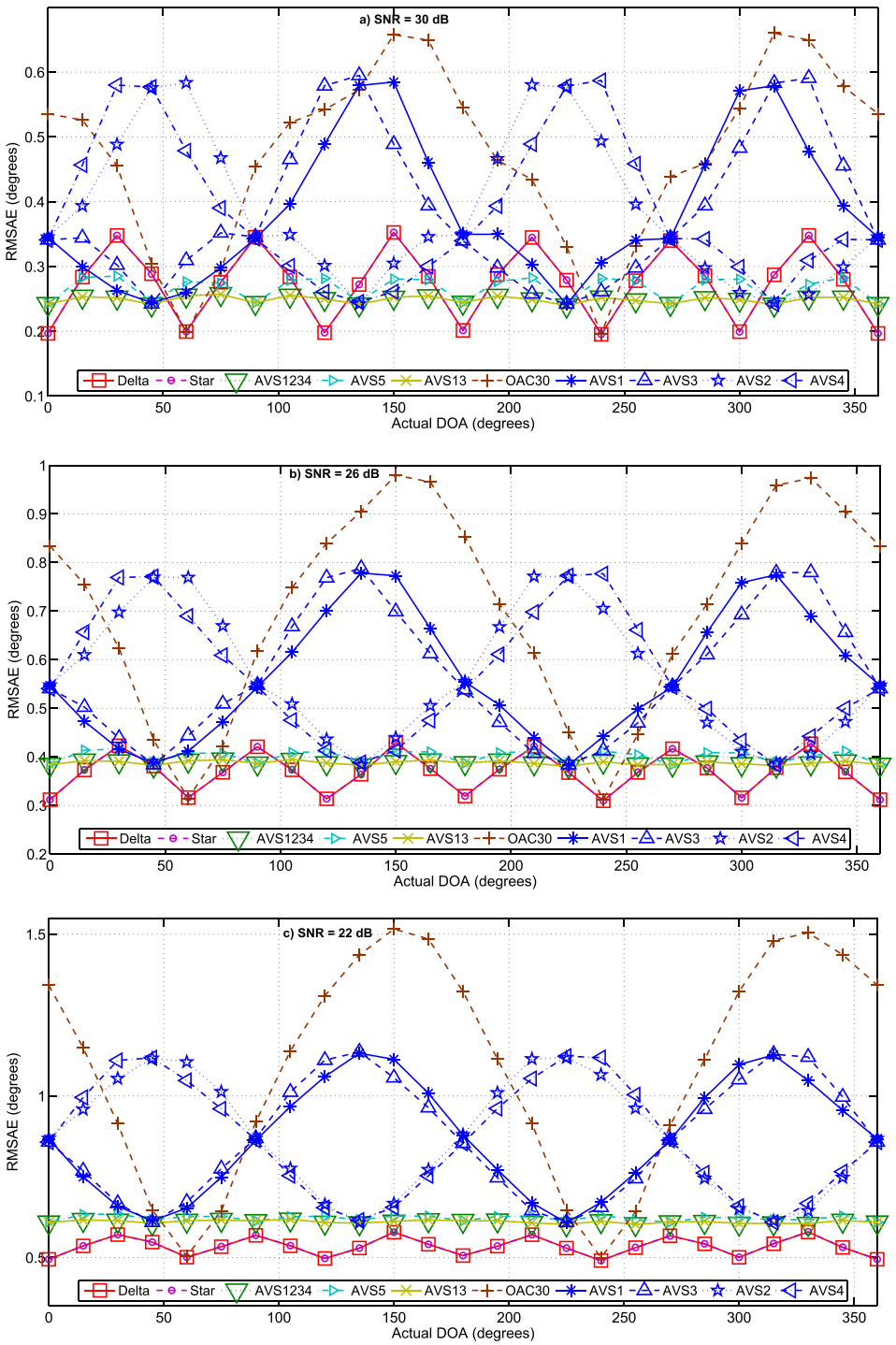

FIG. 6. (Color online) RMSAE versus DoAs for different AVS configurations when sound source is at a range of 1 m and emits 1 kHz sinusoidal signal of 25 ms duration with (a) SNR = 30 dB, (b) SNR = 26 dB, (c) SNR = 22 dB, (d) SNR = 18 dB, (e) SNR = 14 dB, and (f) SNR = 10 dB. Note: The vertical scales of all the graphs are different for better depiction.

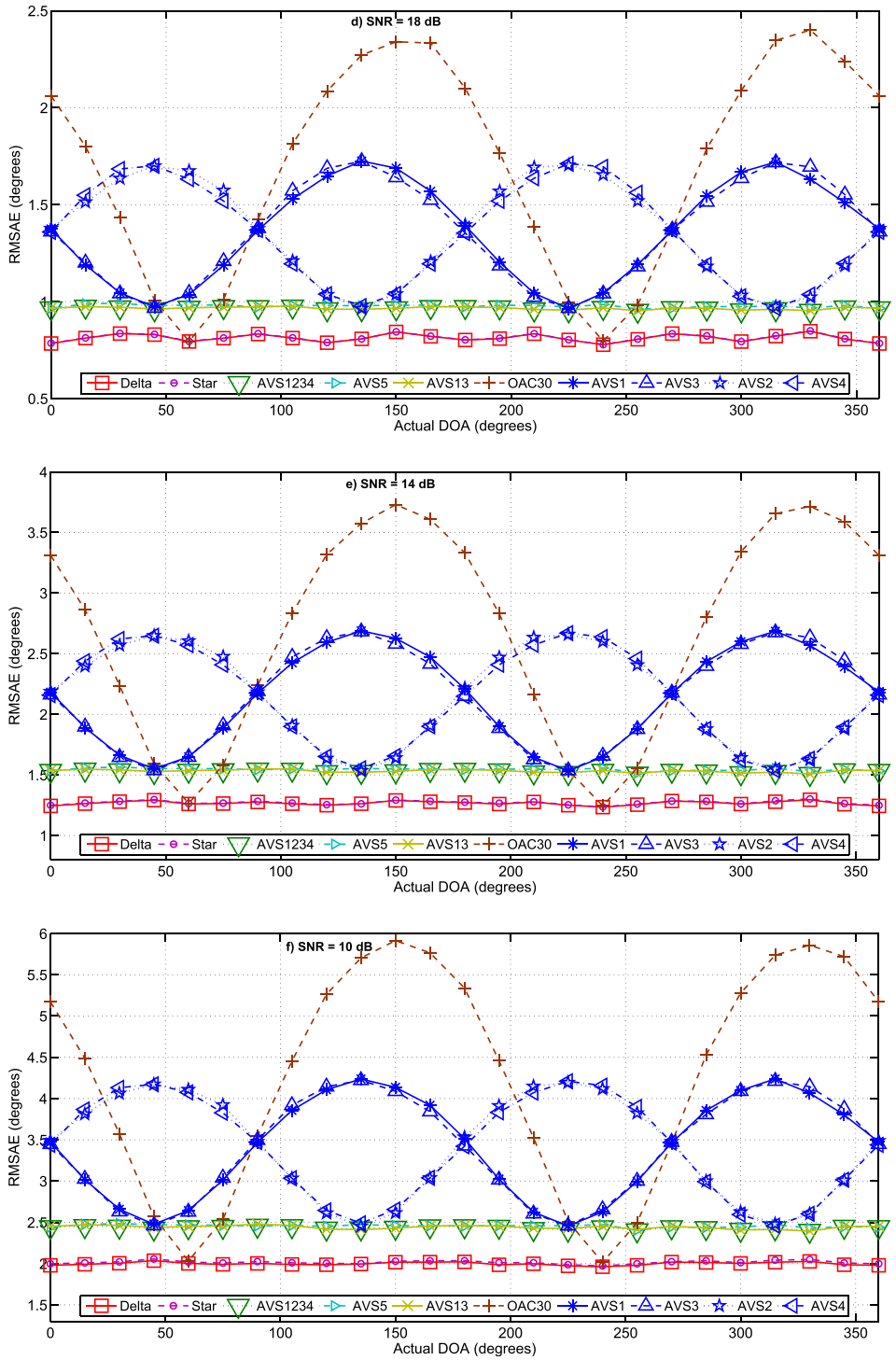

FIG. 6. (Color online) (*Continued*)

VI. EXPERIMENTAL SETUP AND RESULTS

A. Experimental setup

In the experimental setup, identical omni-directional microphones (Sennheiser MKE-1 make, Sennheiser, Germany) of 3.3 mm diameter with sensitivity of 5 mV/Pa at 1 kHz have been used to form the two AVS configurations as shown in Fig. 7. The microphone separations are 16 and 19 mm for the square and the configuration, respectively. Here, we will compare the results of the experiment performed in full-anechoic room with the FEM simulation results of non-zero size microphones (3.3 mm in diameter). For these two configurations, the FEM simulation setup for non-zero size microphone is similar to the experimental set-up. In order to have minimal disturbance in the sound field due to reflections, the microphone supporting structure is made of thin steel rods of $\sim$1 mm diameter, in which each microphone is held by a steel rod as shown in the sketch in Fig. 7. The experiments have

TABLE VI. $\overline{\text{RMSAE}}_{0^\circ:345^\circ}$ (degrees) for various AVS configurations ($d = 10$ mm) under different SNR for sinusoidal source of 1 kHz of 25 ms duration at a range of 1 m.

	$\overline{\text{RMSAE}}_{0^\circ:345^\circ}$ in degrees									
SNR (dB)	Delta	Star	AVS1	AVS2	AVS3	AVS4	OAC30	AVS13	AVS1234	AVS5
Infinity	0.173	0.173	0.151	0.153	0.154	0.151	0.194	0.048	0.048	0.093
30	0.277	0.277	0.386	0.387	0.387	0.385	0.472	0.248	0.248	0.267
26	0.370	0.370	0.568	0.568	0.568	0.566	0.701	0.387	0.387	0.401
22	0.538	0.535	0.869	0.869	0.869	0.867	1.079	0.610	0.610	0.622
18	0.813	0.814	1.358	1.358	1.357	1.355	1.693	0.965	0.965	0.977
14	1.267	1.267	2.144	2.142	2.142	2.138	2.670	1.532	1.530	1.545
10	1.999	2.001	3.407	3.407	3.404	3.404	3.399	2.440	2.435	2.456

been performed in an acoustic full-anechoic room having a lower cutoff frequency of 150 Hz and internal dimensions of 3.34 m × 3.04 m × 2.06 m. The output of the microphones is connected to a high pass filter (Sennheiser make MZA-900-P) which attenuates frequencies below 125 Hz whose output is amplified using a preamplifier (Behringer Ultragain Pro Mic-200, Behringer, Germany). The amplified signal is digitized using a multi-channel data acquisition system (PXI-e 1062Q chassis with PXI 6132 DAQ, National Instruments, Austin, TX) with sampling frequency of 48 kHz and filtered with a low pass filter having pass band and stop band frequency of 4 kHz and 4.5 kHz, respectively. The one second sinusoidal sound source signal of 1 kHz is input to a loudspeaker (M-Audio AV-40) using the NI Digital-to-analog converter. For each angular location considered for the sound source, i.e., 0°, 15°, 30°, 45°, 60°, 75°, and 90°, 100 experiments have been performed to estimate the DoA of the sound source.

B. Experiment results and comparison with simulation results

Figures 8 and 9 show the DoA performance (both experiment and FEM simulation) for three configurations, i.e., delta, and AVS13 and AVS5 configurations, respectively, using a 1 kHz sound source located at a distance of 1 m for different DoAs. The experimental results have been compared with the FEM simulation results for the non-zero size microphone (3.3 mm in diameter) case and are found to follow a similar trend. The RMSAE of the experimental results for the delta configuration are less than 0.052° at the 45° and 60° DoAs, as in the case of non-zero size microphone simulation. One of the possible reasons of the deviation of the results at 0° and 90° for the non-zero size microphone FEM simulation and anechoic room experiments, from FEM simulation of zero-size microphone could be the effect of reflections and diffraction from the microphone body. For AVS13 and AVS5 configurations, the RMSAE is minimum at 0°, 45°, and 90° for the non-zero size microphone simulation case, whereas the experimental results at 0° and 90° vary from the expected zero value. The deviation of the experimental results from the expected results at 0° and 90° are likely due to sources of error from microphone misalignment in its configuration, reflection and diffraction from the microphone body, sensor noise, electrical phase mismatch between the microphones.

TABLE VII. $\overline{\text{RMSAE}}_{0^\circ:345^\circ}$ (degrees) for various configurations as AVS and microphone-array ($d = 10$ mm), aperture size for delta and square are 17.32 mm and 14.14 mm, respectively, and sound source emits 1 kHz signal at a range of 1 m.

	$\overline{\text{RMSAE}}_{0^\circ:345^\circ}$ in degrees						
	AVS			Microphone-array			
	Intensity vector based			MUSIC		GCC	
SNR (dB)	Delta	Star	AVS5	Delta	Square	Delta	Square
30	0.277	0.277	0.267	0.270	0.547	1.169	1.200
26	0.370	0.370	0.401	0.361	0.801	1.420	1.529
22	0.538	0.535	0.622	0.539	1.289	1.837	2.029
18	0.813	0.814	0.977	0.861	2.245	2.625	2.996
14	1.267	1.267	1.545	1.583	4.601	4.358	5.077
10	1.999	2.001	2.456	3.235	8.960	7.908	9.391

VII. CONCLUSION

The paper reports analysis of several AVS microphone configurations for P-P method based DoA estimation in 2-D space. We have investigated the performance of different microphone arrangements as air acoustic vector-sensor configuration for DoA estimation of a radiating source. The mathematical expressions of the DoA estimate in terms of the PSD for various AVS microphone configurations are presented. The numerical simulation using FEM tool considering ideal zero-size as well as practical non-zero size microphones are performed and its results are supported by experiments with a prototype AVS. The performance analysis has encompassed variation of (a) angle of arrival, (b) microphone separation, (c) signal duration, and (d) SNR. It has been identified that the four microphone star-configuration and the three microphone delta-configuration give identical performance in the presence as well as in the absence of noise. Also, the rate of increase in error for these configurations with respect to microphone separation is less than the other configurations considered. An advantage of the delta-configuration is that it requires one less microphone compared to the star-configuration. Also, it has been observed that the four-microphone configurations, viz., AVS13 and AVS1234 give minimum AE in the absence of additive noise with zero-size microphones. However, in the

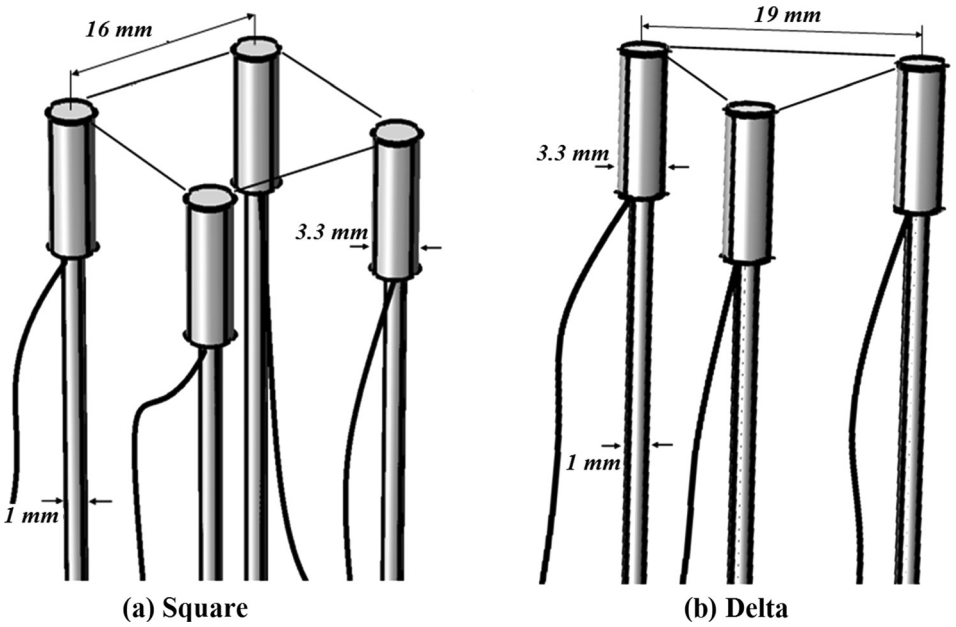

FIG. 7. Sketch for two different AVS structures using microphone placement in 2-D geometry, (a) square and (b) delta.

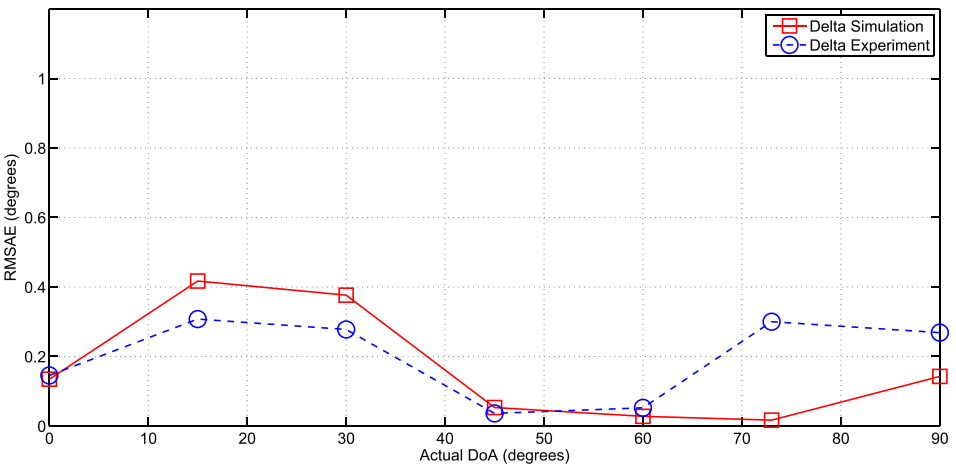

FIG. 8. (Color online) RMSAE comparison of experiment and simulation performance (considering non-zero size microphones) for delta configuration when sound source is at a range of 1 m and emits 1 kHz sinusoidal signal of 1 s duration.

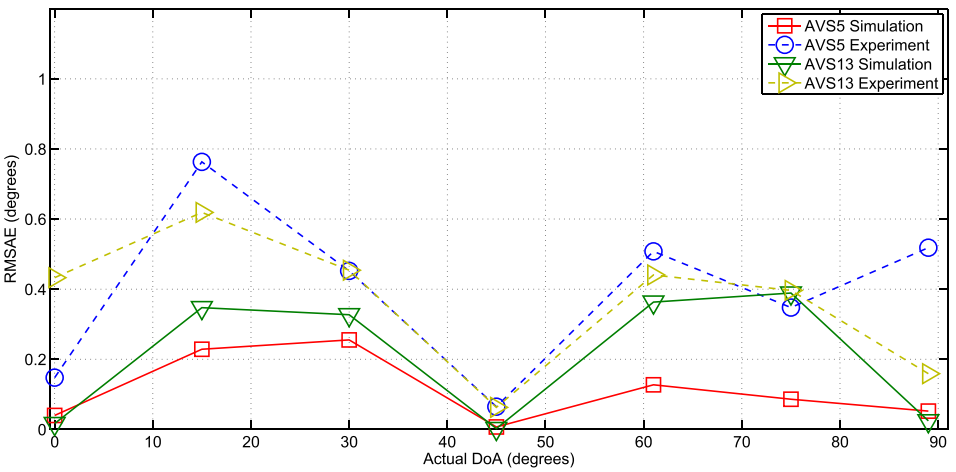

FIG. 9. (Color online) RMSAE comparison of experiment and simulation performance (considering non-zero size microphones) for AVS13 and AVS5 configuration when sound source is at a range of 1 m and emits 1 kHz sinusoidal signal of 1 s duration.

presence of additive noise, the three-microphone configurations, viz., delta and star have lower RMSAE than the other microphone configurations. For example, the $\overline{\text{AAE}}_{0^\circ:345^\circ}$ of the AVS13 and AVS1234 and the delta and star configurations are 0.048° and 0.173°, respectively, for the noise-free case. In the presence of noise, for 10 dB SNR, the four-microphone configurations, i.e., AVS13, AVS123, and AVS5 give an $\overline{\text{RMSAE}}_{0^\circ:345^\circ}$ of 2.4° and the three-microphone configurations, i.e., delta and star give an $\overline{\text{RMSAE}}_{0^\circ:345^\circ}$ of 1.9°. Further, these vector-sensor configurations were also compared to the standard microphone-array based direction-finding methods, i.e., MUSIC and GCC. The FEM simulation performance results show an improvement over these standard microphone-array based methods for SNR ranging from 30 to 10 dB except for delta configurations, which shows improvement below 18 dB SNR. The experiments are performed for delta, AVS13 and AVS5 configurations and the results are compared with the FEM simulation of non-zero size microphone configuration, the trend of the experimental results is same as the FEM simulation except at few angular locations, that could be attributed errors due to practical considerations.

ACKNOWLEDGMENT

The authors thank the anonymous reviewers for their comments and suggestions that have significantly improved the quality of the manuscript.

[1]M. R. Bai, S.-W. Juan, and C.-C. Chen, "Particle velocity estimation based on a two-microphone array and kalman filter," J. Acoust. Soc. Am. **133**(3),1425–1432 (2013).
[2]D. Fernáandez Comesaña, J. Wind, A. Grosso, and K. Holland, "Performance of pp and pu intensity probes using scan and paint," in *International Congress on Sound and Vibrations, ICSV*, Rio de Janeiro, Brazil (2011).
[3]M. T. Silvia and R. T. Richards, "A theoretical and experimental investigation of low-frequency acoustic vector sensors," in *OCEANS'02 MTS/IEEE* (2002), Vol. 3, pp. 1886–1897.
[4]K. H. Miah and E. L. Hixon, "Design and performance evaluation of a broadband three dimensional acoustic intensity measuring system," J. Acoust. Soc. Am. **127**(4), 2338–2346 (2010).
[5]L. E. Kinsler, A. R. Frey, A. B. Coppens, and J. V. Sanders, *Fundamentals of Acoustics*, 4th ed. (Wiley, New York, 1999), pp. 560.
[6]H.-E. De Bree, "The microflown: An acoustic particle velocity sensor," Acoust. Australia **31**(3), 91–94 (2003).
[7]M. W. Thompson and A. A. Atchley, "Simultaneous measurement of acoustic and streaming velocities in a standing wave using laser Doppler anemometry," J. Acoust. Soc. Am. **117**(4), 1828–1838 (2005).
[8]A. Henning, S. Kröber, and L. Koop, "Acoustic particle velocity measurements: A cross comparison between modern sensor technologies," Meas. Sci. Technol. **24**(8), 085303 (2013).
[9]J. K. Thompson and D. R. Tree, "Finite difference approximation errors in acoustic intensity measurements," J. Sound Vib. **75**(2), 229–238 (1981).
[10]F. J. Fahy, "Measurement of acoustic intensity using the cross-spectral density of two microphone signals," J. Acoust. Soc. Am. **62**(4), 1057–1059 (1977).
[11]M. Shujau, C. H. Ritz, and I. S. Burnett, "Designing acoustic vector sensors for localization of sound sources in air," in *EUSIPCO 2009* (2009).
[12]G. Moschioni, B. Saggin, and M. Tarabini, "Sound source identification using coherence- and intensity-based methods," IEEE Trans. Instrum. Meas. **56**(6), 2478–2485 (2007).
[13]B. Gunel, H. Hacihabiboglu, and A. M. Kondoz, "Intensity vector direction exploitation for exhaustive blind source separation of convolutive mixtures," in *IEEE International Conference on Acoustics, Speech and Signal Processing* (2009), pp. 41–44.
[14]X. Zhong, X. Chen, W. Wang, A. Alinaghi, and A. B. Premkumar, "Acoustic vector sensor based reverberant speech separation with probabilistic time-frequency masking," in *2013 Proceedings of the 21st European Signal Processing Conference (EUSIPCO)* (2013), pp. 1–5.
[15]Y. X. Zou, W. Shi, B. Li, C. H. Ritz, M. Shujau, and J. Xi, "Multisource doa estimation based on time-frequency sparsity and joint inter-sensor data ratio with single acoustic vector sensor," in *2013 IEEE International Conference on Acoustics, Speech and Signal Processing (ICASSP)* (2013), pp. 4011–4015.
[16]D. G. Manolakis, V. K. Ingle, and S. M. Kogon, *Statistical and Adaptive Signal Processing: Spectral Estimation, Signal Modeling, Adaptive Filtering, and Array Processing* (Artech House, Norwood, MA, 2005), Vol. 46.
[17]K. Wu, V. G. Reju, and A. W. H. Khong, "Multi-source direction-of-arrival estimation in a reverberant environment using single acoustic vector sensor," in *2015 IEEE International Conference on Acoustics, Speech and Signal Processing (ICASSP)* (2015), pp. 444–448.
[18]Y. Song and K. T. Wong, "Three-dimensional localization of a near-field emitter of unknown spectrum, using an acoustic vector sensor corrupted by additive noise of unknown spectrum," IEEE Trans. Aerospace Electron. Syst. **49**(2), 1035–1041 (2013).
[19]X. Yuan, J. Huang, and R. Calderbank, "Polynomial-phase signal direction-finding and source-tracking with a single acoustic vector sensor," in *2015 IEEE International Conference on Acoustics, Speech and Signmal Processing (ICASSP)* (IEEE, 2015), pp. 2559–2563.
[20]J. C. Shipps and K. Deng, "A miniature vector sensor for line array applications," in *Proceedings of OCEANS 2003* (2003), Vol. 5, pp. 2367–2370.
[21]M. E. Lockwood and D. L. Jones, "Beamformer performance with acoustic vector sensors in air," J. Acoust. Soc. Am. **119**(1), 608–619 (2006).
[22]D. P. Jarrett, E. A. P. Habets, and P. A. Naylor, "Eigenbeam-based acoustic source tracking in noisy reverberant environments," in *2010 Conference Record of the Forty Fourth Asilomar Conference on Signals, Systems and Computers (ASILOMAR)* (2010), pp. 576–580.
[23]M. Shujau, C. H. Ritz, and I. S. Burnett, "Using in-air acoustic vector sensors for tracking moving speakers," in *2010 4th International Conference on Signal Processing and Communication Systems (ICSPCS)* (2010), pp. 1–5.
[24]M. Shujau, C. H. Ritz, and I. S. Burnett, "Speech dereverberation based on linear prediction: An acoustic vector sensor approach," in *2013 IEEE International Conference on Acoustics, Speech and Signal Processing (ICASSP)* (2013), pp. 639–643.
[25]S. Nagata, K. Furihata, T. Wada, D. K. Asano, and T. Yanagisawa, "A three-dimensional sound intensity measurement system for sound source identification and sound power determination by ln modelsa)," J. Acoust. Soc. Am. **118**(6), 3691–3705 (2005).
[26]P. G. Craven and M. A. Gerzon, "Coincident microphone simulation covering three dimensional space and yielding various directional outputs," U.S. patent 4,042,779 (August 16, 1977).
[27]J. Wind, H.-E. de Bree, and B. Xu, "3D sound source localization and sound mapping using a pu sensor array," in *Proceedings of CEAS-AIAA* (2010).
[28]A. Nehorai and E. Paldi, "Acoustic vector-sensor array processing," IEEE Trans. Signal Processing **42**(9), 2481–2491 (1994).
[29]M. Hawkes and A. Nehorai, "Acoustic vector-sensor correlations in ambient noise," IEEE J. Oceanic Eng. **26**(3), 337–347 (2001).
[30]D. Levin, E. A. P. Habets, and S. Gannot, "Maximum likelihood estimation of direction of arrival using an acoustic vector-sensor," J. Acoust. Soc. Am. **131**(2), 1240–1248 (2012).
[31]D. Levin, E. A. P. Habets, and S. Gannot, "On the angular error of intensity vector based direction of arrival estimation in reverberant sound fields," J. Acoust. Soc. Am. **128**(4), 1800–1811 (2010).
[32]P. K. Tam and K. T. Wong, "Cramér-Rao bounds for direction finding by an acoustic vector sensor under nonideal gain-phase responses, noncollocation, or nonorthogonal orientation," IEEE Sensors J. **9**(8), 969–982 (2009).
[33]X. Yuan, "Direction-finding with a misoriented acoustic vector sensor," IEEE Trans. Aerosp. Electron. Syst. **48**(2), 1809–1815 (2012).
[34]Y. Song and K. T. Wong, "A lower bound of direction-of-arrival estimation for an acoustic vector sensor subject to sensor breakdown," IEEE Trans. Aerosp. Electron. Syst. **48**(4), 3703–3708 (2012).
[35]B. Hochwald and A. Nehorai, "Identifiability in array processing models with vector-sensor applications," IEEE Trans. Signal Processing **44**(1), 83–95 (1996).

[36]J. Y. Chung, "Cross-spectral method of measuring acoustic intensity without error caused by instrument phase mismatch," J. Acoust. Soc. Am. **64**(6), 1613–1616 (1978).
[37]G. Krishnappa, "Cross-spectral method of measuring acoustic intensity by correcting phase and gain mismatch errors by microphone calibration," J. Acoust. Soc. Am. **69**(1), 307–310 (1981).
[38]J. H. Rinford, "Technical review to advance techniques in acoustical: Electrical and mechanical measurements" (Bruel and Kjær, Naerum, Denmark, 1981), Vol. 2, no. 3.
[39]S. Doclo, W. Kellermann, S. Makino, and S. E. Nordholm, "Multichannel signal enhancement algorithms for assisted listening devices: Exploiting spatial diversity using multiple microphones," IEEE Signal Processing Mag. **32**(2), 18–30 (2015).
[40]C. Knapp and G. C. Carter, "The generalized correlation method for estimation of time delay," IEEE Trans. Acoust. Speech Signal Processing **24**(4), 320–327 (1976).
[41]R. O. Schmidt, "Multiple emitter location and signal parameter estimation," IEEE Trans. Antennas Propag. **34**(3), 276–280 (1986).